INTERNATIONAL JOURNAL FOR NUMERICAL METHODS IN FLUIDS, VOL. 15, 1025–1036 (1992)

STEPWISE INCREASE IN THE STROUHAL NUMBER FOR FLOWS AROUND FLAT PLATES

SHIGEHIRA OZONO, YUJI OHYA AND YASUHARU NAKAMURA
Research Institute for Applied Mechanics, Kyushu University, Kasuga 816, Japan

AND

RYUZO NAKAYAMA
National Technical College of Kitakyushu, Kitakyushu 803, Japan

SUMMARY

The unsteady viscous flow around flat plates with square leading and trailing edges is investigated by using a finite difference computation of the incompressible two-dimensional Navier–Stokes equations. The chord-to-thickness ratio of a plate ranges from $d/h = 3$ to 9, with a Reynolds number based on the plate's thickness equal to 10^3. The numerical analysis confirms the finding obtained in our previous experiment that vortex shedding from flat plates with square leading and trailing edges is caused by the impinging shear layer instability. The Strouhal number based on the plate's chord increases stepwise with increasing d/h in accordance with the experiment. The numerical analysis also gives some crucial information on the complicated vortical flow occurring near the trailing edge. Finally, the mechanism of the impinging shear layer instability is discussed in the light of the experimental and numerical findings.

KEY WORDS Finite difference method Flat plate Vortex shedding Strouhal number

1. INTRODUCTION

There have been only a few studies of vortex shedding from elongated bluff cylinders[1] in spite of its considerable importance in practical applications associated with flow-induced structural vibrations. In our previous experiment[2] on vortex shedding from flat plates with square leading and trailing edges and chord-to-thickness ratios $d/h = 3$–16, where d is the chord and h is the thickness, at Reynolds numbers of $(1–3) \times 10^3$, it was pointed out that vortex shedding from flat plates is governed by an impinging shear layer instability. This is a kind of single-layer flow instability. In general, it can be caused in some situations where a separated shear layer impinges upon a rigid corner. The separated shear layer created at the upstream corner becomes unstable to roll-up in discrete vortices in the presence of the downstream corner. The length from separation to impingement determines the fundamental scale of vortices and the Strouhal number based on the length often takes a value of around 0·6. In accordance with these general features, our experiment shows that the Strouhal number $St(d)$ based on the plate's chord d was roughly constant and equal to 0·6 for $d/h = 3$–5. With further increase in d/h up to 15, it increased stepwise and the values for each step were roughly equal to integral multiples of 0·6. Although our experimental findings have shed new light on the nature of vortex shedding from flat plates, some problems remain to be understood more clearly and extensively. The purpose of the present study

0271–2091/92/211025–12$11.00 *Received March 1992*

is to observe the time development of the vortex shedding in detail by using a direct finite difference computation and to discuss the mechanism of the stepwise variation in $St(d)$. We have analysed unsteady viscous flows around flat plates with $d/h = 3$–9 at a Reynolds number of 10^3. The incompressible two-dimensional unsteady Navier–Stokes equations were solved in a generalized co-ordinate system using a third-order upwind scheme for the convection term. The computed results have been compared with those of our previous experiment.

2. FORMULATION

To normalize dimensional values, the time $\tilde{t}$, the velocity $\tilde{\mathbf{v}}$ and the pressure $\tilde{p}$, we assumed

$$t = \tilde{t}U/h, \qquad p = \tilde{p}/\rho U^2, \qquad \mathbf{v} = \tilde{\mathbf{v}}/U,$$

where U is the upstream velocity, ρ is the density and h is the height of a flat plate. Thus the two-dimensional governing equations for the incompressible viscous flow can be written in the dimensionless form

$$D\mathbf{v}/d\tilde{t} = -\text{grad}p + (1/Re)\nabla^2\mathbf{v}, \tag{1}$$

$$\text{div}\,\mathbf{v} = 0, \tag{2}$$

with the Reynolds number defined as $Re = Uh/v$, where v is the kinematic viscosity.

Figure 1 shows a typical boundary-fitted grid used in the present computation. By solving a Poisson equation in terms of grid points, we controlled these grids to have grid points concentrated near the body surface.[3] A co-ordinate transformation is introduced in order to

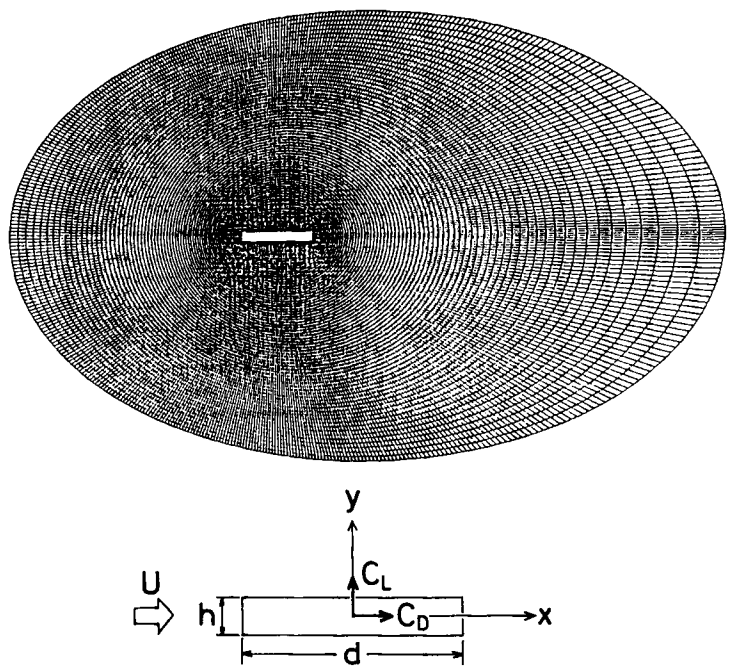

Figure 1. Typical grid system (for a flat plate with $d/h = 8$, 435×81 grid points) and co-ordinate system

distribute a sufficient number of grid points in the boundary layer and the wake as follows:

$$x = x(\xi, \eta), \tag{3a}$$

$$y = y(\xi, \eta), \tag{3b}$$

where (x, y) denotes the original physical domain and (ξ, η) denotes the computational domain. The space derivatives in (3) are written as

$$\frac{\partial}{\partial x} = \left(y_\eta \frac{\partial}{\partial \xi} - y_\xi \frac{\partial}{\partial \eta} \right) \Big/ J, \qquad \frac{\partial}{\partial y} = \left(-x_\eta \frac{\partial}{\partial \xi} + x_\xi \frac{\partial}{\partial \eta} \right) \Big/ J, \qquad \text{etc.,} \tag{4}$$

where $J = x_\xi y_\eta - x_\eta y_\xi$. Both the velocity and pressure are defined at identical points of the mesh system.

The boundary condition used is as follows: the flow velocity $\mathbf{v} = (0, 0)$ on the body surface; $\mathbf{v} = (1, 0)$ on the outer boundary; the pressure p is extrapolated by substitution of $\mathbf{v} = (0, 0)$ into equation (1) on the body surface; p is linearly extrapolated on the outer boundary. The initial condition is taken all over the computational domain as follows: $\mathbf{v} = (0, 0)$; $p = 0$.

The governing equations of motion (1) and (2) are solved with a procedure based on the marker-and-cell (MAC) method.[4] Taking the divergence of equation (1) leads to a Poisson equation for the pressure:

$$\nabla^2 p = -\operatorname{div}(\mathbf{v} \cdot \nabla)\mathbf{v} + (1/Re)\nabla^2(\operatorname{div} \mathbf{v}) - \partial(\operatorname{div} \mathbf{v})/\partial t. \tag{5}$$

The space derivatives are approximated with central differences. The time derivative is approximated with a forward difference:

$$\nabla^2 p^{n+1} = -\operatorname{div}[(\mathbf{v}^n \cdot \nabla)\mathbf{v}^n] + (1/Re)\nabla^2 D^n + D^n/\Delta t, \tag{6}$$

where $D = \operatorname{div} \mathbf{v}$, Δt is the time increment and n is the time step. Although the third term on the right-hand side of equation (5) is zero analytically, it is left in equation (6) to preclude the accumulation of numerical errors owing to the self-adjustment of this corrective term. The Euler implicit scheme is used for the time integration of the equations of motion (1):

$$(\mathbf{v}^{n+1} - \mathbf{v}^n)/\Delta t + (\mathbf{v}^n \cdot \nabla)\mathbf{v}^{n+1} = -\operatorname{grad} p^{n+1} + (1/Re)\nabla^2 \mathbf{v}^{n+1}. \tag{7}$$

Note that the convection terms are linearized as follows: $(\mathbf{v} \cdot \nabla)\mathbf{v} \approx (\mathbf{v}^n \cdot \nabla)\mathbf{v}^{n+1}$. All the space derivatives except the convection terms are approximated with central differences. The convection terms are approximated with a third-order upwind scheme[5] whose leading error is estimated to be $(\Delta x)^3 |f| \partial^4 u/\partial x^4$, where Δx is a grid size and f is an arbitrary function. We solved the finite difference equations (6) and (7) by the successive over relaxation (SOR) iterative method. The Reynolds number Re is assumed to be 10^3 and the time increment Δt is $(1\text{–}2) \times 10^{-3}$ for any case.

For the flat plate with a long chord it is necessary to put a large number of grid lines in the ξ-direction to keep the grid resolution. The outer boundary is about 20 h–50 h upstream and 50 h–110 h downstream from the centre of a flat plate and about 25 h–50 h away in the vertical direction. In the following calculations, various grid sizes are employed for different flat plates. Table I shows the total number of grid points for each plate. We made some preliminary calculations by using different grid systems to investigate the influence of the grid systems on the flow itself, changing the total number of grid points and degree of concentration. Then it was confirmed that the adopted grid systems are valid to investigate vortical structures in the vicinity of flat plates. All the numerical calculations in this work were carried out on the computer systems FACOM-780/20 and FACOM VP-200 at Kyushu University. The typical CPU time required increased with increasing d/h, e.g. 2 h approximately for a plate with $d/h = 3$ and 24 h for $d/h = 9$.

Table I. Grid sizes: i, ξ-direction; j, η-direction

d/h	3	4	5	6	7	8	9
i	209	261	313	365	417	453	505
j	81	81	81	81	81	81	81

3. RESULTS AND DISCUSSION

3.1. *Flow patterns and time histories of lift*

Figures 2 and 3(a) show time histories of the lift coefficient C_L and flow patterns around the flat plates for $d/h=3$, 6 and 9. Figure 3(a) shows that all the flow patterns look like the regular

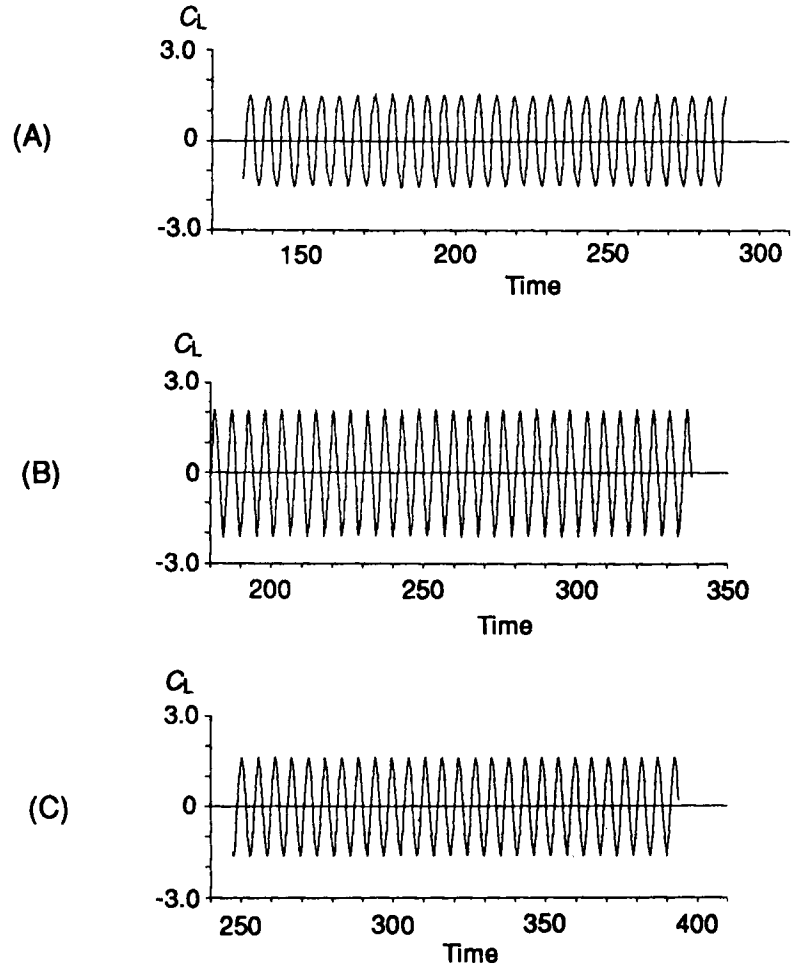

Figure 2. Time histories of lift coefficient C_L for flat plates: (A) $d/h=3$; (B) $d/h=6$; (C) $d/h=9$

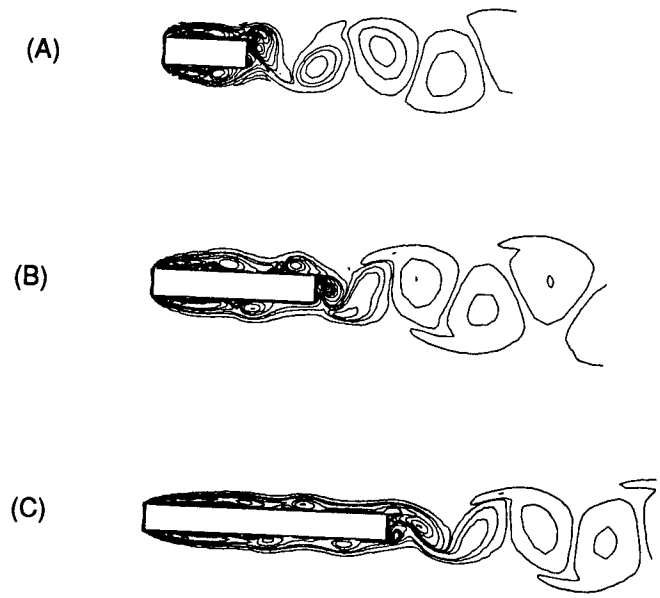

Figure 3(a). Distribution of vorticity around flat plates: (A) $d/h=3$; (B) $d/h=6$; (C) $d/h=9$

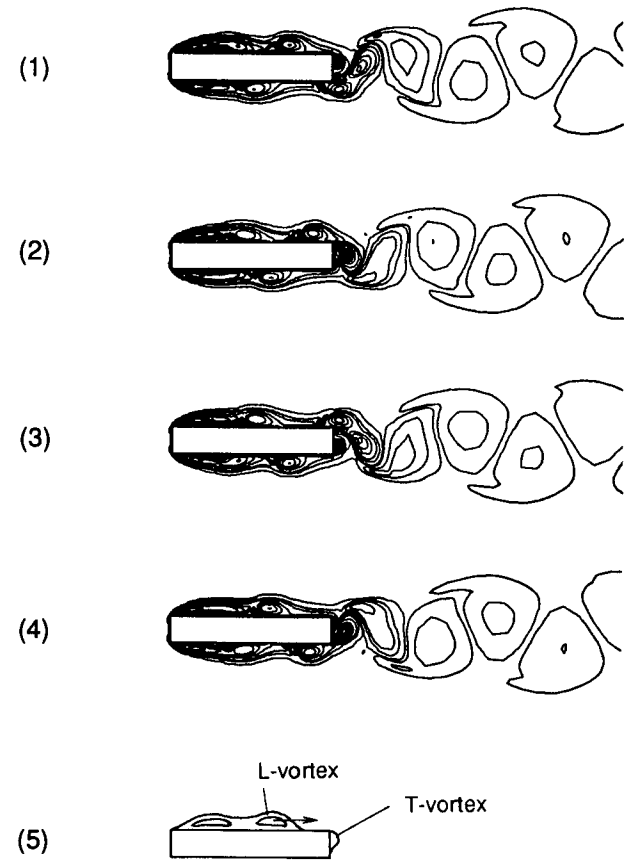

Figure 3(b). Time development of vorticity contours for a flat plate with $d/h=6$: (1)–(4) vorticity contours; (5) descriptive sketch

Karman vortex street. The sinusoidal variations of C_L in Figure 2 confirm this regular vortex shedding. The computed values of $St(d)$ based on the plate's chord for $d/h=3$, 6 and 9 are 0·52, 1·10 and 1·63 respectively. Note that the ratio of the values is roughly 1:2:3.

Figure 3(b) shows the time development of the vortex shedding for $d/h=6$. The shear layer

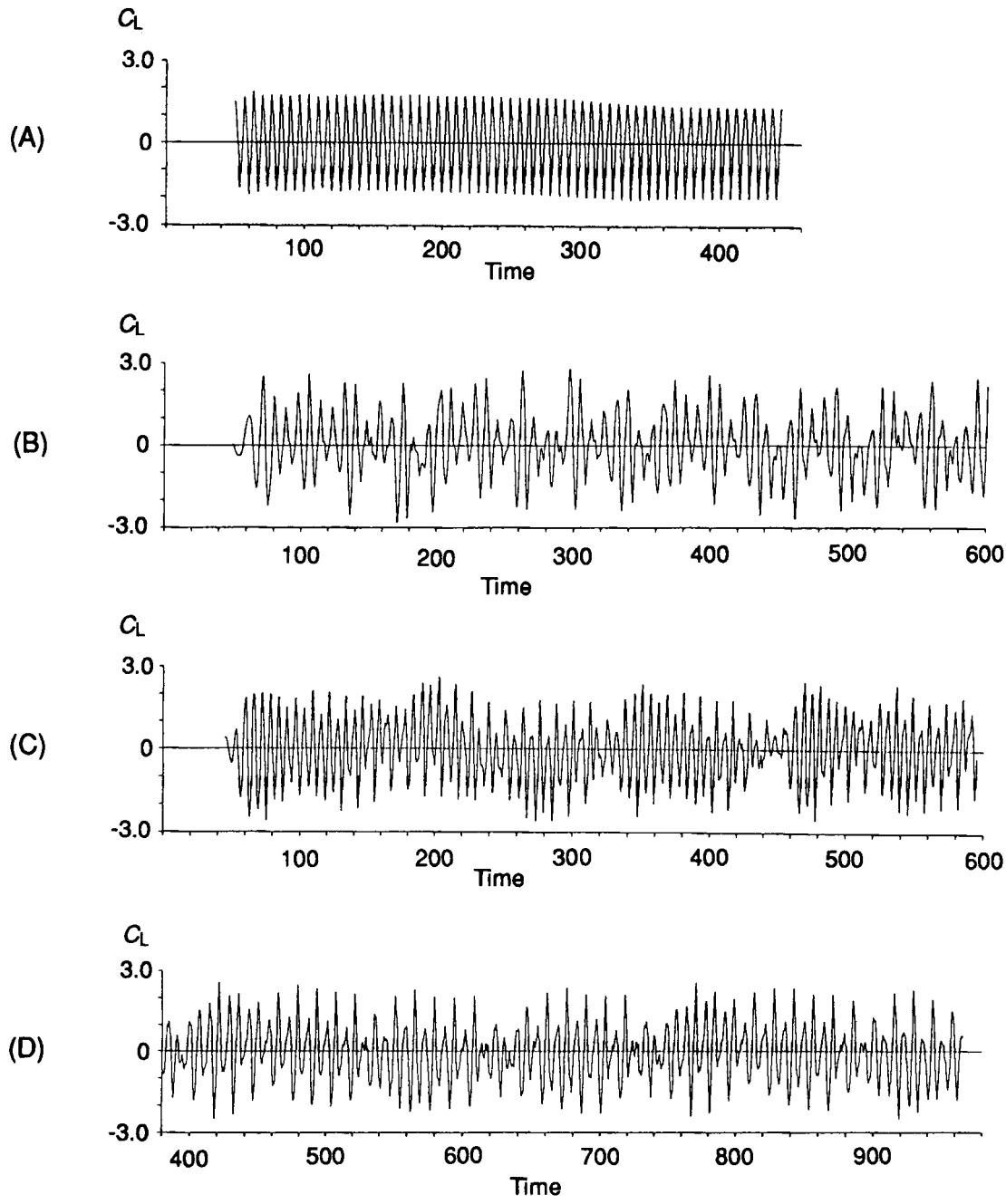

Figure 4. Time histories of lift coefficient C_L for flat plates: (A) $d/h=4$; (B) $d/h=5$; (C) $d/h=7$; (D) $d/h=8$

separating from the leading edge reattaches to a side face and forms a separation bubble. The bubble oscillates in length at the same frequency as the vortex-shedding frequency. The bubble increases steadily in length until the bounding shear layer deflects towards the surface and reattaches half-way along the bubble. The bubble is split into two parts: the upstream one beginning to grow again and the downstream one convecting along a side face as a discrete vortex. The latter is called the L-vortex for brevity. Before the L-vortex reaches the trailing edge, the reattached boundary layer separates again at the trailing edge to form another vortex, which is called the T-vortex for brevity. The T-vortex interacts regularly with the oncoming L-vortex and they are shed in a pair into the downstream wake. The interaction occurs alternately at both upper and lower trailing edge corners. Thus a regular vortex street develops in the downstream wake, thereby producing the regular variations of C_L shown in Figure 2.

Figure 4 shows time variations of C_L and Figure 5(a) shows flow patterns for $d/h=4$, 5, 7 and 8. In contrast to $d/h=3$, 6 and 9, the vortex shedding for $d/h=4$, 5, 7 and 8 is irregular in accordance with the irregular fluctuations of C_L presented in Figure 4; although a time variation for $d/h=4$, exceptionally, seems closely sinusoidal, the time-averaged value is apparently shifting.

Figure 5(b) shows the time development of the vortex shedding for $d/h=8$. In a different way from Figure 3(b), imperfect pairing of L- and T-vortices can be seen at a trailing edge, where L- and T-vortices are shed separately from the trailing edge. The source of the irregularity in C_L

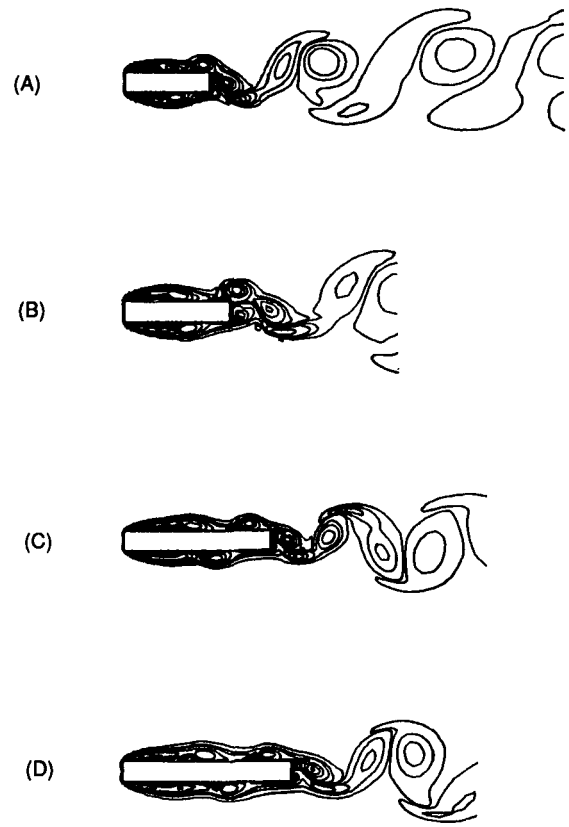

Figure 5(a). Vorticity contours around flat plates: (A) $d/h=4$; (B) $d/h=5$; (C) $d/h=7$; (D) $d/h=8$

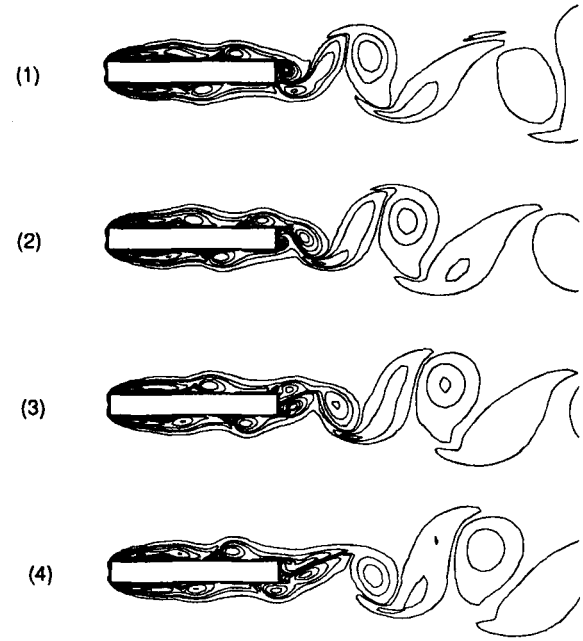

Figure 5(b). Time development of vorticity contours for a flat plate with $d/h=8$

can be attributed to the timing of shedding of the L- and T-vortices at the upper and lower trailing edge corners.

It should be noted that in the process of vortex shedding, only one vortex is formed on a side face for a sequence of $d/h=3$–5 as shown in Figures 3 and 5. Similarly, two vortices are formed for a sequence of $d/h=6$–8 and three vortices for $d/h=9$. Thus the numbers of vortices formed on a side face coincide with the ratio of the computed Strouhal numbers $St(d)$, i.e. 1:2:3.

Despite this common feature for each sequence, there are apparent differences in both the time variations of C_L and the flow patterns. If we observe a specific sequence of flow patterns, e.g. $d/h=6$–8, we can find differences among them. The flow for the smallest d/h, i.e. $d/h=6$, is thought to be, so to speak, the basic flow in the sequence, because the flow shows a regular interaction between the vortex shed from upstream and the vortex formed on the back face. However, as d/h increases, this kind of regular interaction breaks down and a complicated interaction emerges. It is likely that the interaction controls the downstream vortical structure and gives rise to the irregularities.

3.2. Strouhal number

The computed Strouhal number $St(d)$ based on the plate's chord against d/h is presented in Figure 6, which includes the results of our previous experiment.[2] The computed Strouhal number increases stepwise with d/h and its values are roughly equal to integral multiples of 0·6 in a similar way to those of the experiment. Figures 3(a) and 5(a) show that the number of vortices formed on a side face increases in correspondence with the stepwise increase in the Strouhal number. The ratio of the Strouhal numbers coincides with the number of vortices formed on a side face. Thus the numerical analysis confirms that the vortex shedding from flat plates is characterized by the

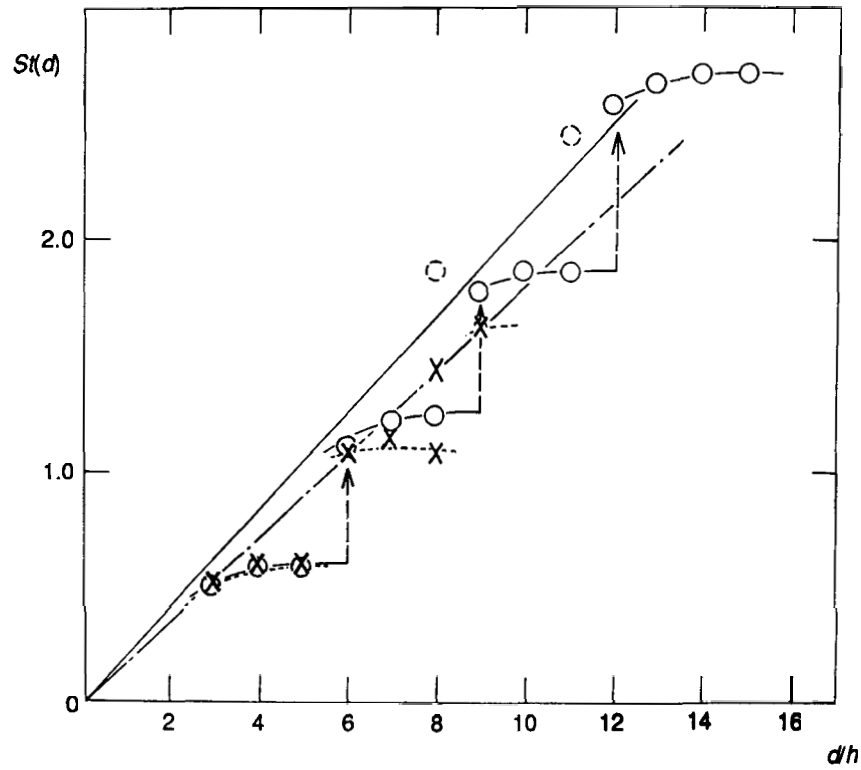

Figure 6. Strouhal number $St(d)$ based on the chord versus chord-to-thickness ratio d/h at $Re=10^3$: ○, experimental (taken from Reference 2); ×, numerical

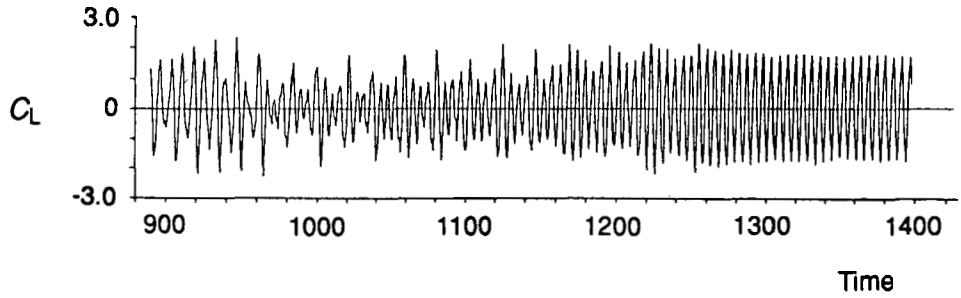

Figure 7. Time history of lift coefficient C_L for a transitional $d/h=8$

impinging shear layer instability. Flat plates with $d/h=3$–5 can be classified into the first mode, similarly those with $d/h=6$–8 are classified into the second mode, and so on.

Returning to Figure 6, it is seen that the computed Strouhal number takes multiple values at $d/h=8$ in a similar manner to the experiment. Figure 7 shows a part of the time history of the lift coefficient for $d/h=8$. In an earlier stage, there are irregular fluctuations. However, as time proceeds, a regular sinusoidal variation appears spontaneously. The flow pattern (a) in

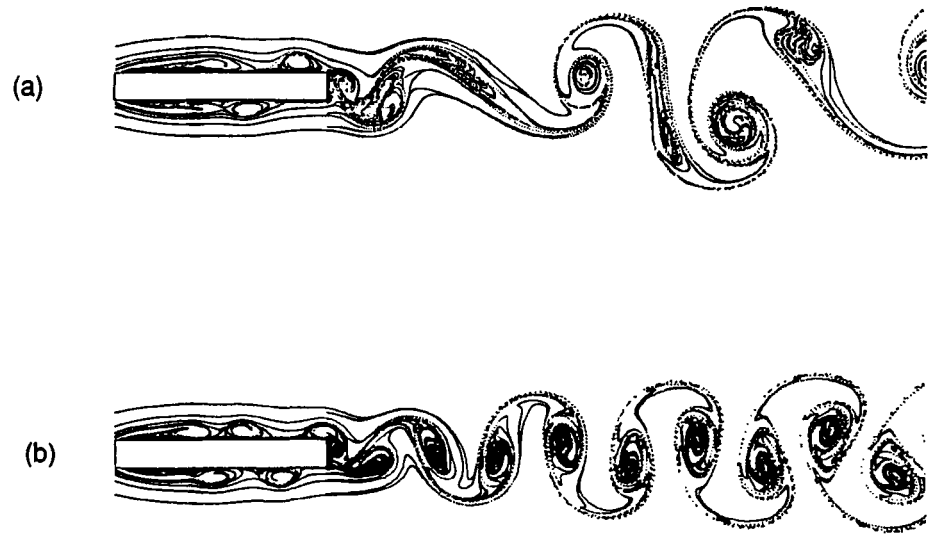

Figure 8. Streaklines for a transitional $d/h = 8$: (a) the lower $St(d) = 1{\cdot}2$, second mode; (*b*) the higher $St(d) = 1{\cdot}8$, third mode

Figure 8 corresponds to the irregular stage and the flow pattern (b) to the regular stage. What is interesting is that the pattern (a) has two vortices on a side face but the pattern (b) has three vortices, and the ratio of the Strouhal numbers is roughly 2:3. In other words, the multiple values at $d/h = 8$ indicate a transition from the second mode to the third mode.

We observed these two kinds of modes also in a laboratory experiment. Flow visualization using liquid paraffin smoke was conducted in a wind tunnel with a rectangular working section 2 m high, 4 m wide and 6 m long. A flat plate with $d/h = 8$ was mounted at zero incidence across the centre of the working section. The flow velocity was $1\ \mathrm{m\,s^{-1}}$ to obtain the same Reynolds number as in the computation, i.e. $Re = 10^3$. Figures 9(a) and 9(b) show instantaneous side views of the flow around the plate. As shown in Figure 9(a), two vortices are present on a side face. On the other hand, Figure 9(b) shows three vortices on a side face. The ratio of the Strouhal number is roughly 2:3. These results are in good agreement with the numerical results.

3.3. Impinging shear layer instability

According to Rockwell and Naudascher,[6] the shear layer instability is greatly enhanced by the feedback control of the impinging edge on the vorticity production at the separation point. We also think that the trailing edge of the flat plates plays an essential role of enhancing the shear layer instability.

The impinging shear layer instability starts at about $d/h = 3$ where the wavelength of vortex shedding is nearly equal to the plate's chord. As d/h is increased, the wavelength is locked on to the plate's chord through some non-linear flow processes until a certain limit is reached. At the limit, transition of the mode of vortex shedding from $n = 1$ to $n = 2$ occurs, as has been reproduced for a flat plate with $d/h = 8$ by using a finite difference computation in the preceding subsection. With a further increase in d/h the same cycle of events repeats itself. Thus the stepwise variation of the Strouhal number appears for the flow around the flat plates.

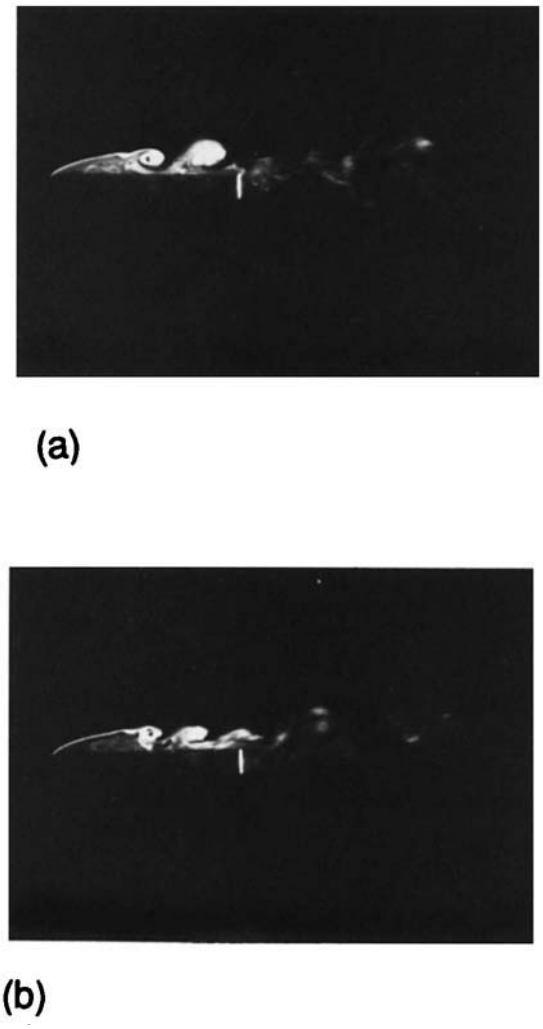

Figure 9. Visualization of the flow around a flat plate with $d/h=8$ at $Re=10^3$: (a) side view, second mode, $St(d)=1{\cdot}2$, (b) side view, third mode, $St(d)=1{\cdot}8$

4. CONCLUSIONS

The viscous incompressible flow around flat plates with square leading and trailing edges was investigated by using the finite difference computation of the unsteady Navier–Stokes equations at $Re=10^3$. The chord-to-thickness ratio of a flat plate ranged from $d/h=3$ to 9. The results are as follows.

The vortex shedding from flat plates with $d/h=3$–9 is governed by the impinging shear layer instability. This is because the computed Strouhal number increases stepwise with d/h and the values are roughly equal to integral multiples of 0·6 in a similar way to that of the experiment. The ratio of the Strouhal numbers is 1:2:3 in accordance with the number of vortices formed on a side face.

If we observe a sequence of flow patterns of a specific mode, some differences can be seen among them. The flow for the smallest d/h is, so to speak, the basic flow which shows a regular interaction between the vortex shed from the upstream corner and the vortex formed on the back face. As d/h increases, this kind of regular interaction breaks down, with irregularities in vortex shedding emerging. With further increase in d/h the flow jumps to that of a higher mode. There is a complicated interaction between the vortex shed from upstream and that formed on the back face which controls the downstream vortical flow. The source of the irregularities in the flow may be attributed to the interaction.

REFERENCES

1. Y. Nakamura and M. Nakashima, 'Vortex excitation of prisms with elongated rectangular, H and T cross-sections', *J. Fluid Mech.*, **163,** 149–169 (1986).
2. Y. Nakamura, Y. Ohya and H. Tsuruta, 'Experiments on vortex shedding from flat plates with square leading and trailing edges', *J. Fluid Mech.*, **222,** 437–447 (1991).
3. J. F. Thompson, F. C. Thames and C. W. Mastin, 'Boundary fitted curvilinear coordinate systems for solution of partial differential equations on fields containing any number of arbitrary two-dimensional bodies', *NASA CR-2729*, 1977.
4. F. H. Harlow and J. E. Welch, 'Numerical calculation of time dependent viscous incompressible flow of fluid with free surface', *Phys. Fluids*, **8,** 2182–2189 (1965).
5. T. Kawamura and K. Kuwahara, 'Computation of high Reynolds number flow around a circular cylinder with surface roughness', *AIAA Paper 84-0340*, 1984.
6. D. Rockwell and E. Naudascher, 'Review—Self-sustaining of flow past cavities', *Trans. ASME. I: J. Fluids Eng.*, **100,** 152–165 (1978).